

# Energy storage properties and electrocaloric effect of $\text{Ba}_{0.65}\text{Sr}_{0.35}\text{TiO}_3$ ceramics near room temperature

Peng-Zu Ge<sup>1</sup> · Xin-Gui Tang<sup>1</sup> · Qiu-Xiang Liu<sup>1</sup> · Yan-Ping Jiang<sup>1</sup> · Wen-Hua Li<sup>1</sup> · Jie Luo<sup>1</sup>

Received: 8 September 2017 / Accepted: 7 October 2017 / Published online: 14 October 2017  
© Springer Science+Business Media, LLC 2017

**Abstract**  $\text{Ba}_{0.65}\text{Sr}_{0.35}\text{TiO}_3$  (BST) ceramics were synthesized by sol–gel route. The diffusion phase transition (DPT) characteristic was found in the temperature range from 150 to  $-35$  °C. The value of the DPT parameter  $\gamma$  values are 1.53 and 1.75, respectively at applied dc field of 0 and 16.7 kV/cm. It is implied that the phase transition of BST ceramics become more diffuse under the applied electric field. Temperature dependent polarization–electric field hysteresis loops were studied. It was found that the energy storage properties and electrocaloric effect near room temperature were the function of electric fields. The maximum value of recoverable energy density was  $0.2812 \text{ J/cm}^3$  with energy storage efficiency ( $\eta$ ) of 78.67% obtained at room temperature under an electric field of 75 kV/cm. The largest  $\eta$  can achieve 98% under low electric field of 50 kV/cm. A large electrocaloric temperature change ( $\Delta T_{\text{max}} = 0.49 \text{ K}$ ) near room temperature was obtained by indirect method. Taken together, the ceramics have a promising candidate for energy-storage applications and cooling systems in the room temperature.

## 1 Introduction

Investigated material,  $(\text{Ba},\text{Sr})\text{TiO}_3$ , is known as a classic lead-free relaxor. Because of the environmental and health concerns related to lead of people, BST has attracted significant attentions as strong candidates for application in

multilayer ceramic capacitors [1], dynamic random-access memory, tunable microwave devices [2, 3] and piezoelectric transducers [4] instead of lead materials. Recently, with the increasing demand for energy efficiency and the development of cooling technology, the study of energy storage and electrocaloric effect (ECE) in  $(\text{Ba},\text{Sr})\text{TiO}_3$  ceramics has been in the spotlight. Generally, there are many ways to store energy, such as batteries, electrochemical capacitors, dielectric capacitors [5], and so on. In fields where huge power is required, ceramic capacitors with large power density are necessary [6]. Enhancing breakdown strength (BDS) can obtain large energy storage density, which needs high consistency with least number of pores [7]. One of the ways is to decrease the sintering temperature of bulk ceramics, such as liquid phase sintering, spark plasma sintering (SPS) [8], doping oxides or compounds with low melting points ( $\text{CuO}$ ,  $\text{Li}_2\text{CO}_3$ ,  $\text{V}_2\text{O}_5$ ,  $\text{LiF}$ , etc.), doping glass with low softening points [9], and so on, but doping can lead to low saturation polarization, which is bad for the improvement of energy storage properties [9]. Recently, Shao et al. reported that  $0.9(\text{K}_{0.5}\text{Na}_{0.5})\text{NbO}_3-0.1\text{Bi}(\text{Mg}_{2/3}\text{Nb}_{1/3})\text{O}_3$  ceramics obtained a large energy storage density under high electric field [10]. However, for the practical application, as a lead-free dielectric material for energy storage capacitor, not only high energy storage density but also high energy storage efficiency is desirable [11].

On the other hand, the Electrocaloric (EC) refrigeration based on the ECE has been regarded to possess a promising future instead of existing vapor-cycle refrigeration [12–15]. The ECE is defined as the reversible adiabatic temperature change and/or isothermal entropy change of a dielectric material upon the application or removal of an external electric field. Up to now, many kinds of ferroelectric materials like bulk materials, thin films, thick films, single crystals and polymers were chosen to study ECE [16, 17]. Thin films

✉ Xin-Gui Tang  
xgtang@gdut.edu.cn

<sup>1</sup> School of Physics & Optoelectric Engineering,  
Guangdong University of Technology, Guangzhou  
Higher Education Mega Center, Guangzhou 510006,  
People's Republic of China

usually have a larger ECE than bulk materials, but the small size, low EC strength ( $\Delta T/\Delta E$ ) [16] and low thermal inertia [17] limit the application. On the contrary, bulk materials have a promising candidate for the application in middle and large scale devices [18]. However, many people only pursue larger electrocaloric temperature for bulk materials, which neglect the practical application in room temperature of EC materials, the report of room temperature ECE is less. Therefore, we choose the lead-free  $\text{Ba}_{0.65}\text{Sr}_{0.35}\text{TiO}_3$  ceramics as our research, of which the largest electrocaloric temperature occurs near the room temperature. In this work, the high energy storage efficiency was reported; the room temperature ECE and mechanism of  $\text{Ba}_{0.65}\text{Sr}_{0.35}\text{TiO}_3$  ceramics were also calculated and discussed, respectively.

## 2 Experimental

$\text{Ba}_{0.65}\text{Sr}_{0.35}\text{TiO}_3$  (abbreviated as BST) ceramics were prepared from powders synthesized by a sol–gel route. High purity barium acetate  $\text{Ba}(\text{CH}_3\text{COO})_2$ , strontium acetate  $\text{Sr}(\text{CH}_3\text{COO})_2 \cdot 1/2\text{H}_2\text{O}$ , titanium *n*-butoxide  $\text{Ti}(\text{OC}_4\text{H}_9)_4$  were selected according to the molecular weight ratio, acetic acid  $\text{CH}_3\text{CH}_2\text{OOH}$  and 2-methoxyethanol ( $\text{C}_3\text{H}_8\text{O}_2$ ) were selected as solvents. The details of powders preparation process were described elsewhere [9]. The powders were dried and pressed into disks. The pellets were sintered at 1320 °C for 5 h and cooled in a furnace. Both sides of the samples were painted with silver paste and sintered at 650 °C for 2 h.

The dielectric permittivity  $\epsilon_r$  and loss tangent  $\tan\delta$  were measured under various dc biases using a blocking circuit, a multifrequency LCR meter (Model SR720 of Stanford Research System, USA), and a dc power source of 1000 V (Keithley 6517A, USA), the temperature from 150 to –35 °C. The crystal structure and orientation of samples were characterized by X-ray diffractometer (XRD). The microstructure was examined by an XL30 FEG (Philips, Eindhoven, The Netherlands) field-emission scanning electron microscope (FE-SEM). The round ceramic samples were 9.40 mm diameter by 0.60 mm thick. Ferroelectric hysteresis loops were obtained by a computer-controlled virtual-ground circuit with Precision Premier II Ferroelectric Tester (Radiant Technologies, Inc., Albuquerque, New Mexico, USA).

## 3 Results and discussion

The XRD pattern is shown in Fig. 1a, There are six obvious diffraction peaks (100), (110), (111), (200), (210), (211) and no secondary phase can be detected, results imply that the BST ceramics exhibit a pure perovskite structure. The SEM image of the BST ceramics is exhibited in the Fig. 1b. It is observed that the grains grow well and the microstructure is

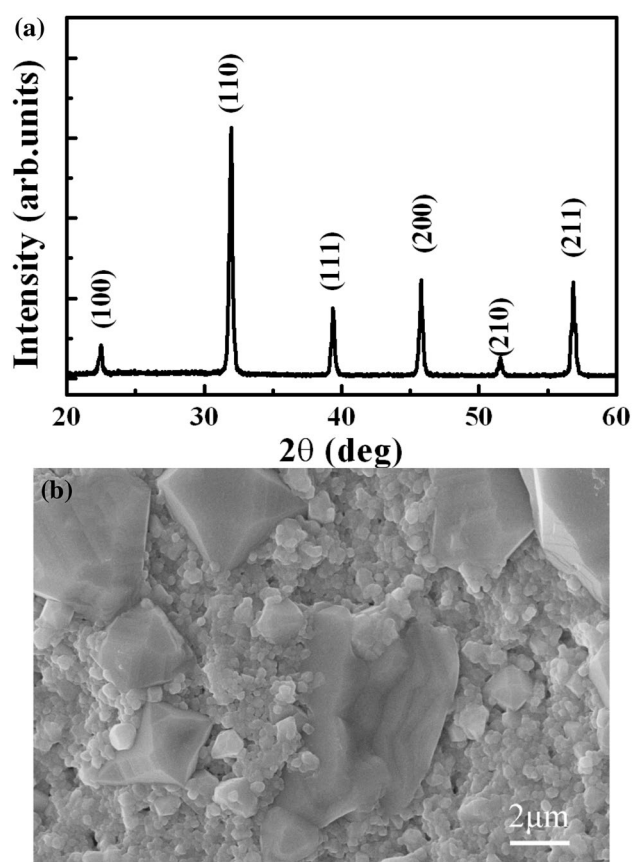


**Fig. 1** a The XRD pattern and b SEM image of BST ceramics

dense. The samples exhibit a good densification with well interconnected grains and without major voids. However, some obviously large grains coexist with the small grains. The reason is that the powders synthesized by a sol–gel route have fine particles and thus tend to agglomerate, the agglomerate particles will grow to large grains at the high temperature, while the particles without agglomerating will normally grow to small grains.

Figure 2a shows the temperature dependence of the dielectric permittivity  $\epsilon_r$  and loss tangent  $\tan\delta$  for the BST samples during cooling under different dc electric fields at various frequencies from 100 Hz to 100 kHz, and 10 kHz, respectively. It is interesting to note that the dielectric peaks of the samples for two dc electric fields are located at the temperature around 16–17 °C (temperature of the maximum dielectric permittivity  $\epsilon_m(T_m)$ ), suggesting the BST ceramics undergo a ferroelectric to relaxor phase transition [19, 20], the results of the Fig. 5a further proves it. Compared with the curve of temperature dependence of  $\epsilon_r$  under 0 kV/cm, the curve for 16.7 kV/cm is low and wide, indicating that the ceramics go through a field-induced phase transition. When the applied electric field is 0 kV/cm, the  $\epsilon_r$  and loss  $\tan\delta$  of the BST ceramics increase from 734 to 0.00158 to 4045 and 0.00845 with the decreased

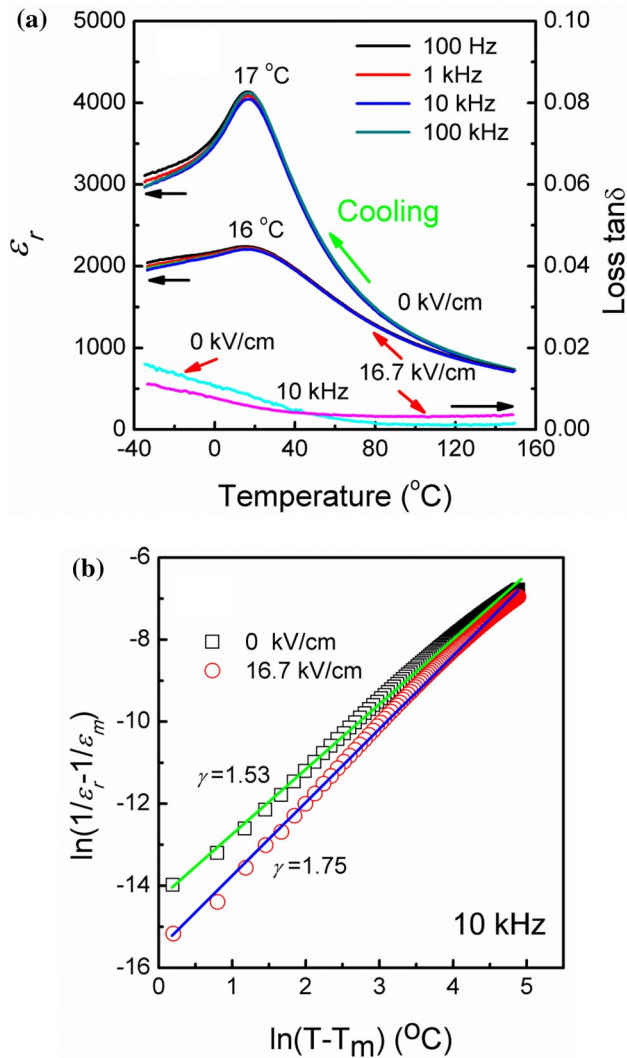


**Fig. 2** **a** The dielectric properties as a function of temperature of BST ceramics and **b** plot of  $\ln(1/\epsilon_r - 1/\epsilon_m)$  as a function of  $\ln(T - T_m)$  for BST ceramics measured at 10 kHz. The solid line was fitted by Eq. (1)

temperature from 150 to 17 °C, respectively, then decrease to 2964 and 0.01596 when temperature decreases to - 35 °C. Oppositely, when the applied electric field is 16.7 kV/cm, the  $\epsilon_r$  and  $\tan\delta$  of the BST ceramics increase from 709 to 0.00367 to 2207 and 0.00598 with the decreased temperature from 149 to 16 °C, respectively, then decrease to 1966 and 0.01112 when temperature decreases to - 34 °C. The dielectric loss of the BST ceramic is lower than 0.01 when temperature is higher than 7 and - 22 °C, respectively applied electric field of 0 and 16.7 kV/cm.

The diffusion characteristics of ferroelectric phase transition could be described by a modified Curie–Weiss relationship [21, 22]:

$$1/\epsilon_\gamma - 1/\epsilon_m = (T - T_m)^\gamma / C_1, \quad (1 \leq \gamma \leq 2) \quad (1)$$

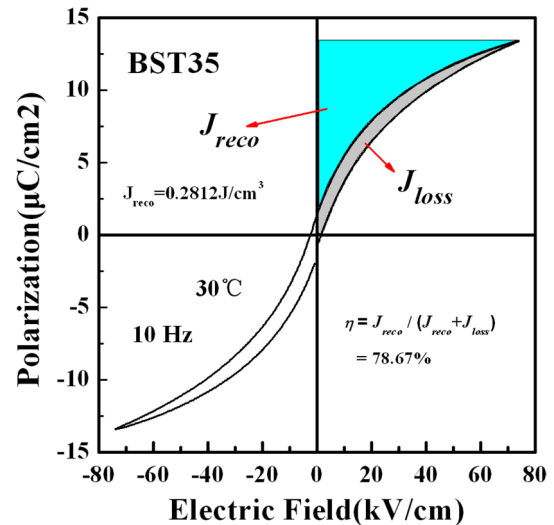


**Fig. 3**  $P$ – $E$  hysteresis loops of BST ceramics measured at room temperature with an electric field of 75 kV/cm

where  $\gamma$  and  $C_1$  were assumed to be constant. The parameter  $\gamma$  gave information on the character of the phase transition: for  $\gamma = 1$ , a normal Curie–Weiss law was obtained,  $\gamma = 2$  described a complete diffuse phase transition [21]. Figure 2(b) showed the plot of  $\ln(1/\epsilon_\gamma - 1/\epsilon_m)$  versus  $\ln(T - T_m)$  at 10 kHz. By fitting the experimental data based on Eq. (1), we obtained the value of parameter  $\gamma = 1.75$ , the values of  $\gamma$  were found to increase from 1.53 to 1.75 with increasing dc field range from 0 to 16.7 kV/cm. It is implied that the phase transition of BST ceramics become more diffuse under the applied electric field. The BST ceramics has the characteristics of the relaxation ferroelectric, and from the Fig. 5a, the spontaneous polarization ( $P_s$ ) is not zero with the temperature rise to 85 °C (over the  $T_m$ ) further proved the relaxor nature.

Figure 3 represents the  $P$ – $E$  hysteresis loop of the BST ceramics measured at room temperature under the electric field of 75 kV/cm. The samples exhibit slim  $P$ – $E$  hysteresis loop. As for the practical use of dielectrics in energy storage devices, energy storage density, energy loss density and energy storage efficiency are important parameters calculated from the hysteretic  $P$ – $E$  loop, wherein the charging and discharging paths are not coincident, energy delivered to the capacitor cannot be release completely [11]. Generally, energy storage properties can be estimated from the integrated area according to the  $P$ – $E$  hysteresis loop. The recoverable energy storage density ( $J_{reco}$ ), energy loss density ( $J_{loss}$ ) and the energy storage efficiency ( $\eta$ ) are calculated on the basis of the formulas as follows:

$$J_{reco} = \int_{P_r}^{P_{max}} EdP \quad (2)$$

$$J_{loss} = \int_0^{P_{max}} EdP - J_{reco} \quad (3)$$

$$\eta = \frac{J_{reco}}{J_{reco} + J_{loss}} \times 100\% \quad (4)$$

where  $E$  is the applied electric field,  $P$  is the polarization,  $P_{max}$  is the maximum polarization corresponding to the maximum experimental electric field and  $P_r$  is the remnant polarization. In this work, the  $J_{reco}$ ,  $J_{loss}$  and  $\eta$  calculated from  $P$ - $E$  hysteresis loop are 0.2812, 0.0762 J/cm<sup>3</sup> and 78.67% respectively for BST ceramics measured at room temperature with the electric field of 75 kV/cm.

Figure 4a shows the variations of  $P$ - $E$  hysteresis loops of the BST ceramics measured at room temperature under various electric fields. It is worth noting that the  $P_{max}$  increase sharply while the  $P_r$  increase slightly with the increase of electric field, demonstrating a much higher energy density can be achieved by improving the dielectric strength of the ceramics [16]. The calculated  $J_{reco}$ ,  $J_{loss}$  and  $\eta$  under different electric fields at room temperature are presented in Fig. 4b. The  $J_{reco}$  increases from 0.0168 to 0.2812 J/cm<sup>3</sup> and the  $J_{loss}$  increases from 0.0023 to 0.0762 J/cm<sup>3</sup> as electric field increase from 10 to 75 kV/cm. The  $\eta$  remains in 78–88%. The maximum of  $J_{reco}$  is higher than other reported BST ceramics under the same electric field (75 kV/cm), such as

SrTiO<sub>3</sub> ceramics (<0.1 J/cm<sup>3</sup>) [23], Ba<sub>0.2</sub>Sr<sub>0.8</sub>TiO<sub>3</sub> ceramics (<0.15 J/cm<sup>3</sup>) [23], Ba<sub>0.3</sub>Sr<sub>0.7</sub>TiO<sub>3</sub> ceramics (<0.2 J/cm<sup>3</sup>) [23, 24], Ba<sub>0.4</sub>Sr<sub>0.6</sub>TiO<sub>3</sub> ceramics (<0.25 J/cm<sup>3</sup>) [23], Ba<sub>0.4</sub>Sr<sub>0.6</sub>TiO<sub>3</sub>-MgO ceramics ( $\leq$ 0.2 J/cm<sup>3</sup>) [25].

Figure 5a reveals the variations of  $P$ - $E$  loops of the BST ceramics measured at different temperatures under the electric field of 50 kV/cm. Both spontaneous polarization ( $P_s$ ) and remanent polarization ( $P_r$ ) decrease with the increasing temperature, but are not zero amply that the polar nanometer regions (PNRs) exist in high temperature. These results certified that relaxor feature. The calculated  $J_{reco}$ ,  $J_{loss}$  and  $\eta$  are shown in Fig. 5b. The  $J_{reco}$  and  $J_{loss}$  values remain in 0.1172–0.1817 and 0.0046–0.0605 J/cm<sup>3</sup>, respectively. Obviously, the  $\eta$  is 98% at 25 °C, which is higher than the previously reported values for lead-free ceramics, such as 0.65BaTiO<sub>3</sub>-0.35Bi<sub>0.5</sub>Na<sub>0.5</sub>TiO<sub>3</sub> ceramics (90%) [11], Ba<sub>0.4</sub>Sr<sub>0.6</sub>Zr<sub>0.15</sub>Ti<sub>0.85</sub>O<sub>3</sub> ceramics with SrO-B<sub>2</sub>O<sub>3</sub>-SiO<sub>2</sub> glass (88.2%) [26], 0.8(K<sub>0.5</sub>Na<sub>0.5</sub>)NbO<sub>3</sub>-0.2Sr(Sc<sub>0.5</sub>Nb<sub>0.5</sub>)O<sub>3</sub>-0.5 mol%ZnO ceramics (73.2%) [27], 0.9CaTiO<sub>3</sub>-0.1BiScO<sub>3</sub> ceramics (90.4%) [28].

The electrocaloric effect (ECE) can be evaluated from the temperature dependent  $P$ - $E$  hysteresis loops. Based on the Maxwell relationship  $(\partial S/\partial E)_T = (\partial P/\partial T)_E$ , the isothermal

**Fig. 4** The electric-field-related **a**  $P$ - $E$  hysteresis loops and **b** energy-storage properties of the BST ceramics

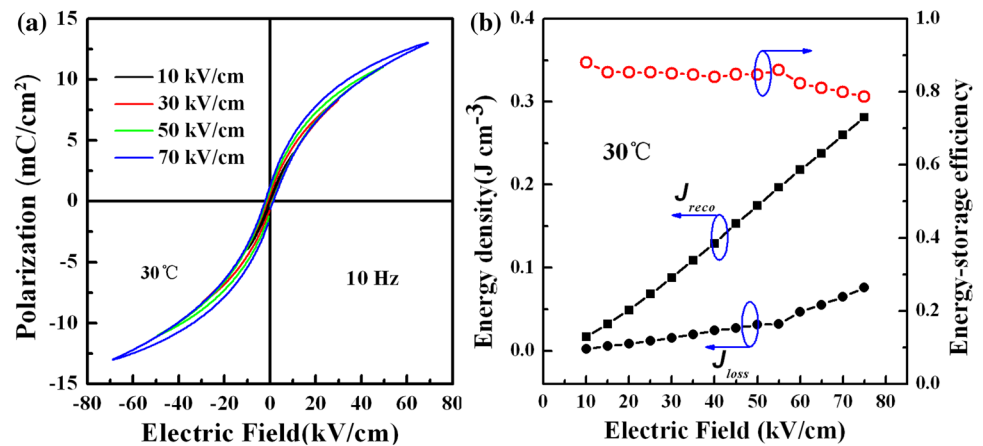
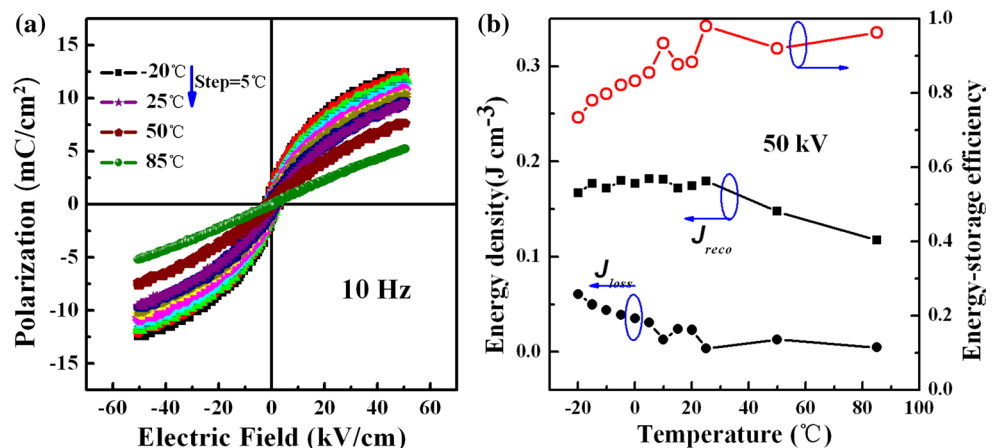


**Fig. 5** The temperature-related **a**  $P$ - $E$  hysteresis loops and **b** energy-storage properties of the BST ceramics





entropy change  $\Delta S$  and adiabatic temperature change  $\Delta T$  can be determined by:

$$\Delta S = -\frac{1}{\rho} \int_{E_1}^{E_2} \left( \frac{\partial P}{\partial T} \right)_E dE \quad (5)$$

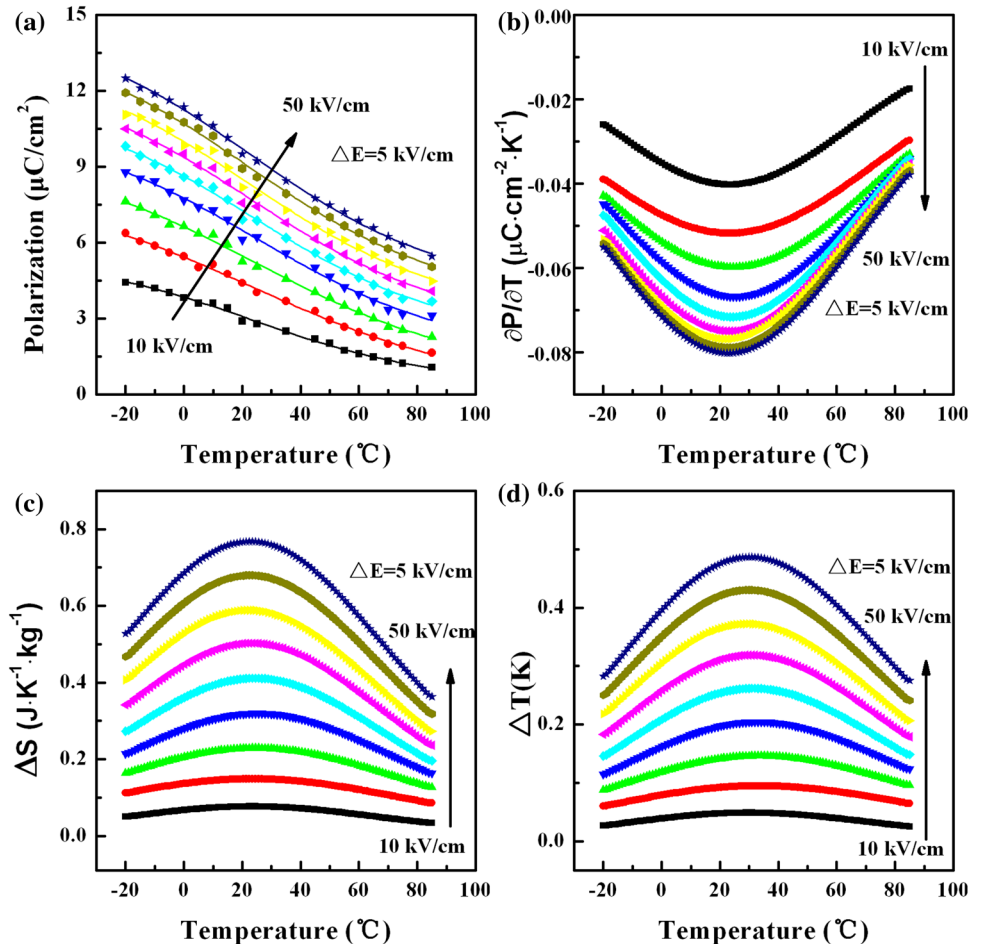
$$\Delta T = -\frac{1}{\rho} \int_{E_1}^{E_2} \frac{T}{C_p} \left( \frac{\partial P}{\partial T} \right)_E dE \quad (6)$$

where  $T$  is the temperature,  $P$  is the polarization,  $\rho$  is the mass density and  $C_p$  is the heat capacity;  $E_1$  and  $E_2$  are the lower and higher applied electric fields, respectively.

Figure 6a displays the variation of the polarization for an applied electric field varying from 10 to 50 kV/cm established from the temperature dependent  $P$ – $E$  hysteresis loops. Using Boltzman nonlinear curves to fit the dots and get the  $P$ – $T$  curves (solid lines in Fig. 6a). The nonlinear curve fittings agree well with the measured data. The values of  $(\partial P/\partial T)_E$  evaluated from the derivative of  $P$ – $T$  curves at different fields are shown in Fig. 6b. An obvious peak is observed in the vicinity of 20 °C attributing to the ferroelectric to paraelectric (FE–PE) phase [9].

$\Delta S$  and  $\Delta T$  are key parameters to evaluate the ECE of a FE material in an ideal refrigeration cycle based on the reported conventional (positive) ECE [29]. For the calculation, the mass density  $\rho$  is measured to be 5.22 g/cm<sup>3</sup> by the Archimedes method using distilled water; the heat capacity is taken as 473 J/(kg·K) [30]. According to Eqs. (4) and (5), the  $\Delta S$  and  $\Delta T$  are plotted in Fig. 6c and d. The peak values of  $\Delta S$  and  $\Delta T$  increase as the  $E$  increases from 10 to 50 kV/cm, which indicates a larger EC value can be obtained at higher electric fields until the electrical breakdown. Therefore, in the practical application, enhancing EC effect can be achieved by increasing the breakdown field, such as hot-pressing [31], spark plasma sintering (SPS) [30], doping a bit glass [32]. The maximum  $\Delta S$  (0.77 J/K kg) is obtained near the Curie temperature  $T_C$  at the applied field of 50 kV/cm. Usually,  $\Delta T$  is maximized near the phase transition, where thermally driven changes in measured polarization  $P$  resulting from changes in the magnitude are largest [33]. However, in our work, the maximum  $\Delta T$  (0.49 K) is obtained near 30 °C, which is higher than  $T_C$ , similar phenomena were also reported in Ba<sub>0.94</sub>Ca<sub>0.06</sub>Ti<sub>1-x</sub>Sn<sub>x</sub>O<sub>3</sub> ceramics [34]. EC is a function of applied electric field, the higher the electric field, the greater the ECE [18]. Under the same as electric

**Fig. 6** Temperature dependent **a** polarization **b** pyroelectric coefficient  $(\partial P/\partial T)$  **c** entropy change  $(\Delta S)$  **d** temperature change  $(\Delta T)$  at different electric fields



field of 50 kV/cm, the BST ceramics show higher value of  $\Delta T$  than that of the lead-free ceramics such as  $\text{Na}_{0.5}\text{Bi}_{0.5}\text{TiO}_3$  (0.33 K) [35],  $0.7(\text{Na}_{0.5}\text{Bi}_{0.5})\text{TiO}_3\text{--}0.3\text{SrTiO}_3$  (<0.4 K) [16],  $\text{Bi}_{0.5}\text{Na}_{0.5}\text{TiO}_3\text{--BaTiO}_3\text{--}(\text{Sr}_{0.7}\text{Bi}_{0.2}\square_{0.1})\text{TiO}_3$  (<0.4 K) [36],  $\text{SrBi}_{1.85}\text{Pr}_{0.15}(\text{Nb}_{0.2}\text{Ta}_{0.8})_2\text{O}_9$  ceramics (<0.45 K) [37].

To compare the ECEs of different materials at different electrical fields, the electrocaloric strength ( $\Delta T/\Delta E$ ) is calculated. For industrial applications, a large EC efficiency is crucial for exploring suitable lead-free electrocaloric materials [34]. The electrocaloric strength is defined as the ratio between the EC temperature change and the strength of the electric field inducing the effect [38]. The electrocaloric strength of 0.01 K cm/kV for BST ceramics is obtained at  $E = 50$  kV/cm.

Generally, a large ECE in normal ferroelectrics with a first-order phase transition usually occurs in the vicinity of a narrow temperature with ferroelectric–paraelectric phase transition. However, for relaxor ferroelectric ceramics, the phase transition is wide and diffuse, so the large ECE with wide temperature range in practical use is preferred [39–41]. Li et al. reported that a considerable  $\Delta T$  value can be maintained over a wide temperature range well above the temperature of the pseudo-first-order phase transition under a high electric field in  $\text{Bi}_{0.5}\text{Na}_{0.5}\text{TiO}_3$ -based relaxor ferroelectric ceramics. They also pointed out the ECE is closely related to the structural phase transition and electric field strength [19]. Therefore, if the electric field strength is large enough, the ECE temperature change of BST ceramics will be larger than the values predicted under low electric field in this work.

## 4 Conclusion

In this work, temperature dependent dielectric and ferroelectric properties of the BST ceramics were studied. The value of the diffusion phase transition parameter  $\gamma$  values are 1.53 and 1.75, respectively applied dc field of 0 and 16.7 kV/cm, indicated the diffusion phase transition features. The energy storage properties of BST ceramics with different electric fields and temperatures were revealed. The energy storage density of 0.2812 J/cm<sup>3</sup> and energy storage efficiency of 78.67% under the electric field of 75 kV/cm can be obtained at room temperature (30 °C). It was worth noting that the largest  $\eta$  of 98% was achieved at 25 °C under the electric field of 50 kV/cm. The ECE of BST ceramics was also investigated by the indirect method. Electrocaloric temperature change of 0.49 K and electrocaloric strength of 0.01 K cm/kV for BST ceramics were obtained at room temperature under the electric field of 50 kV/cm. Although the energy storage properties and ECE were not very satisfactory, this work provides a guide for the design of energy storage and ECE materials around room temperature.

**Acknowledgements** This work was supported by the National Natural Science Foundation of China (Grant Nos. 11574057 and 51604087), the Guangdong Provincial Natural Science Foundation of China (Grant No. 2016A030313718), and the Science and Technology Program of Guangdong Province of China (Grant Nos. 2016A010104018, and 2017A0104022).

## References

1. H. Saito, H. Chazono, H. Kishi, N. Yamaoka, X7R multilayer ceramic capacitors with nickel electrodes. *Jpn. J. Appl. Phys.* **30**, 2307–2310 (1991)
2. W.J. Kim, W. Chang, S.B. Qadri, J.M. Pond, S.W. Kirchoefer, D.B. Chrisey, J.S. Horwitz, Microwave properties of tetragonally distorted  $(\text{Ba}_{0.5}\text{Sr}_{0.5})\text{TiO}_3$  thin films. *Appl. Phys. Lett.* **76**, 1185–1187 (2000)
3. X.X. Xi, H.C. Li, W.D. Si, A.A. Sirenko, I.A. Akimov, J.R. Fox, A.M. Clark, J.H. Hao, Oxide thin films for tunable microwave devices. *J. Electroceram.* **4**, 393–405 (2000)
4. T.T. Chen, M.S. Fu, B.W. Jia, Y.J. Wu, X.Q. Liu, X.M. Chen, Dielectric and ferroelectric properties of  $\text{Ba}_{1-x}\text{Sr}_x\text{TiO}_3$  ceramics: effects of grain size and ferroelectric domain. *Adv. Appl. Ceram.* **112**, 270–276 (2013)
5. B.B. Liu, X.H. Wang, R.X. Zhang, L.T. Li, Grain size effect and microstructure influence on the energy storage properties of fine-grained  $\text{BaTiO}_3$ -based ceramics. *J. Am. Ceram. Soc.* **100**, 3599–3607 (2017)
6. T.M. Correia, M. McMillen, M.K. Rokosz, P.M. Weaver, J.M. Gregg, G. Viola, M.G. Cain, A lead-free and high-energy density ceramic for energy storage applications. *J. Am. Ceram. Soc.* **96**, 2699–2702 (2013)
7. H.Y. Lee, K.H. Cho, H.-D. Nam, Grain size and temperature dependence of electrical breakdown in  $\text{BaTiO}_3$  ceramic. *Ferroelectrics* **334**, 165–169 (2006)
8. P.R. Ren, Q. Wang, S.F. Li, G.Y. Zhao, Energy storage density and tunable dielectric properties of  $\text{BaTi}_{0.85}\text{Sn}_{0.15}\text{O}_3/\text{MgO}$  composite ceramics prepared by SPS. *J. Eur. Ceram. Soc.* **37**, 1501–1507 (2017)
9. Q.X. Liu, X.G. Tang, Y.Y. Deng, J. Wang, H.L.W. Chan, Nonlinear dielectric properties of sol-gel derived  $(\text{Ba},\text{Sr})\text{TiO}_3$  ceramics. *Mater. Chem. Phys.* **112**, 281–284 (2008)
10. T.Q. Shao, H.L. Du, H. Ma, S.B. Qu, J. Wang, J.F. Wang, X.Y. Wei, Z. Xu, Potassium-sodium niobate based lead-free ceramics: novel electrical energy storage materials. *J. Mater. Chem. A* **5**, 554–563 (2017)
11. H.B. Yang, F. Yan, Y. Lin, T. Wang, L. He, F. Wang, A lead free relaxation and high energy storage efficiency ceramics for energy storage applications. *J. Alloys Compd.* **710**, 436–445 (2017)
12. S. Patel, A. Chauhan, R. Vaish, Caloric effects in bulk lead-free ferroelectric ceramics for solid-state refrigeration. *Energy Technol.* **4**, 244–248 (2016)
13. M. Valant, Electrocaloric materials for future solid-state refrigeration technologies. *Prog. Mater. Sci.* **57**, 980–1009 (2012)
14. X. Moya, S. Kar-Narayan, N.D. Mathur, Caloric materials near ferroic phase transitions. *Nat. Mater.* **13**, 439–450 (2014)
15. S.G. Lu, Q.M. Zhang, Electrocaloric materials for solid-state refrigeration. *Adv. Mater.* **21**, 1983–1987 (2009)
16. W.P. Cao, W.L. Li, X.F. Dai, T.D. Zhang, J. Sheng, Y.F. Hou, W.D. Fei, Large electrocaloric response and high energy-storage properties over a broad temperature range in lead-free NBT-ST ceramics. *J. Eur. Ceram. Soc.* **36**, 593–600 (2016)
17. K.S. Srikanth, R. Vaish, Enhanced electrocaloric, pyroelectric and energy storage performance of  $\text{BaCe}_x\text{Ti}_{1-x}\text{O}_3$ . *J. Eur. Ceram. Soc.* **37**, 3927–3933 (2017)

18. Z. Zhu, X.G. Tang, Y.P. Jiang, Q.X. Liu, T.F. Zhang, Z.Y. Feng, Giant electrocaloric effect in lead zinc niobate titanate single crystal. *J. Alloys Compd.* **710**, 297–301 (2017)
19. F. Li, G.R. Chen, X. Liu, J.W. Zhai, B. Shen, S.D. Li, P. Li, K. Yang, H.R. Zeng, H.X. Yan, Type-I pseudo-first-order phase transition induced electrocaloric effect in lead-free  $\text{Bi}_{0.5}\text{Na}_{0.5}\text{TiO}_3\text{-}0.06\text{BaTiO}_3$  ceramics. *Appl. Phys. Lett.* **110**, 182904 (2017)
20. X.G. Tang, J. Wang, X.X. Wang, H.L.W. Chan, Effects of grain size on the dielectric properties and tunabilities of sol-gel derived  $\text{Ba}(\text{Zr}_{0.2}\text{Ti}_{0.8})\text{O}_3$  ceramics. *Solid State Commun.* **131**, 163–168 (2004)
21. K. Uchino, S. Nomura, Critical exponents of the dielectric constants in diffused-phase-transition crystals. *Ferroelectr. Lett. Sect.* **44**, 55–61 (1982)
22. D. Viehland, M. Wuttig, L.E. Cross, The glassy behavior of relaxor ferroelectrics. *Ferroelectrics* **120**, 71–77 (1991)
23. Y. Wang, Z.Y. Shen, Y.M. Li, Z.M. Wang, W.Q. Luo, Y. Hong, Optimization of energy storage density and efficiency in  $\text{Ba}_x\text{Sr}_{1-x}\text{TiO}_3$  ( $x \leq 0.4$ ) paraelectric ceramics. *Ceram. Int.* **41**, 8252–8256 (2015)
24. Y.J. Wu, Y.H. Huang, N. Wang, J. Li, M.S. Fu, X.M. Chen, Effects of phase constitution and microstructure on energy storage properties of barium strontium titanate ceramics. *J. Eur. Ceram. Soc.* **37**, 2099–2104 (2017)
25. Y.H. Huang, Y.J. Wu, W.J. Qiu, J. Li, X.M. Chen, Enhanced energy storage density of  $\text{Ba}_{0.4}\text{Sr}_{0.6}\text{TiO}_3\text{-MgO}$  composite prepared by spark plasma sintering. *J. Eur. Ceram. Soc.* **35**, 1469–1476 (2015)
26. T. Wu, Y.P. Pu, K. Chen, Dielectric relaxation behavior and energy storage properties in  $\text{Ba}_{0.4}\text{Sr}_{0.6}\text{Zr}_{0.15}\text{Ti}_{0.85}\text{O}_3$  ceramics with glass additives. *Ceram. Int.* **39**, 6787–6793 (2013)
27. B. Qu, H. Du, Z. Yang, Q. Liu, T. Liu, Enhanced dielectric breakdown strength and energy storage density in lead-free relaxor ferroelectric ceramics prepared using transition liquid phase sintering. *RSC Adv.* **6**, 34381–34389 (2016)
28. B.C. Luo, X.H. Wang, E.K. Tian, H.Z. Song, H.X. Wang, L.T. Li, Enhanced energy storage density and high efficiency of lead-free  $\text{CaTiO}_3\text{-BiScO}_3$  linear dielectric ceramics. *ACS Appl. Mater. Interfaces* **9**, 19963–19972 (2017)
29. M. Ye, T. Li, Q. Sun, Z.K. Liu, B.L. Peng, C.W. Huang, P. Lin, S.M. Ke, X.R. Zeng, X. Peng, L. Chen, H.T. Huang, A giant negative electrocaloric effect in Eu-doped  $\text{PbZrO}_3$  thin films. *J. Mater. Chem. C* **4**, 3375–3378 (2016)
30. X.Q. Liu, T.T. Chen, Y.J. Wu, X.M. Chen, Enhanced electrocaloric effects in spark plasma-sintered  $\text{Ba}_{0.65}\text{Sr}_{0.35}\text{TiO}_3$ -based ceramics at room temperature. *J. Am. Ceram. Soc.* **96**, 1021–1023 (2013)
31. G.Z. Zhang, Z.B. Chen, B.Y. Fan, J.G. Liu, M. Chen, M. Shen, P. Liu, Y.K. Zeng, S.L. Jiang, Q. Wang, Large enhancement of the electrocaloric effect in PLZT ceramics prepared by hot-pressing. *APL Mater.* **4**, 064103 (2016)
32. X.S. Qian, H.J. Ye, Y.T. Zhang, H. Gu, X. Li, C. Randall, Q. Zhang, Giant electrocaloric response over a broad temperature range in modified  $\text{BaTiO}_3$  ceramics. *Adv. Funct. Mater.* **24**, 1300–1305 (2014)
33. W.P. Geng, Y. Liu, X.J. Meng, L. Bellaiche, J.F. Scott, B. Dkhil, A.Q. Jiang, Giant negative electrocaloric effect in antiferroelectric La doped  $\text{Pb}(\text{ZrTi})\text{O}_3$  thin films near room temperature. *Adv. Mater.* **27**, 3165–3169 (2015)
34. X.J. Wang, F. Tian, C.L. Zhao, J.G. Wu, Y. Liu, B. Dkhil, M. Zhang, Z.P. Gao, X.J. Lou, Giant electrocaloric effect in lead-free  $\text{Ba}_{0.94}\text{Ca}_{0.06}\text{Ti}_{1-x}\text{Sn}_x\text{O}_3$  ceramics with tunable Curie temperature. *Appl. Phys. Lett.* **107**, 252905 (2015)
35. Y. Bai, G.P. Zheng, S.Q. Shi, Abnormal electrocaloric effect of  $\text{Na}_{0.5}\text{Bi}_{0.5}\text{TiO}_3\text{-BaTiO}_3$  lead-free ferroelectric ceramics above room temperature. *Mater. Res. Bull.* **46**, 1866–1869 (2011)
36. F. Li, G.R. Chen, X. Liu, J.W. Zhai, B. Shen, H.R. Zeng, S.D. Li, P. Li, K. Yang, H.X. Yan, Phase-composition and temperature dependence of electrocaloric effect in lead-free  $\text{Bi}_{0.5}\text{Na}_{0.5}\text{TiO}_3\text{-BaTiO}_3\text{-(Sr}_{0.7}\text{Bi}_{0.2}\text{□}_{0.1})\text{TiO}_3$  ceramics. *J. Eur. Ceram. Soc.* **37**, 4732–4740 (2017)
37. A.K. Axelsson, F. Le Goupil, M. Valant, N.M. Alford, Electrocaloric effect in lead-free aurivillius relaxor ferroelectric ceramics. *Acta Mater.* **124**, 120–126 (2017)
38. M. Sanlialp, V.V. Shvartsman, M. Acosta, D.C. Lupascu, Electrocaloric effect in  $\text{Ba}(\text{Zr,Ti})\text{O}_3\text{-(Ba,Ca)TiO}_3$  ceramics measured directly. *J. Am. Ceram. Soc.* **99**, 4022–4030 (2016)
39. Y. Zhao, X.H. Hao, Q. Zhang, A giant electrocaloric effect of a  $\text{Pb}_{0.97}\text{La}_{0.02}(\text{Zr}_{0.75}\text{Sn}_{0.18}\text{Ti}_{0.07})\text{O}_3$  antiferroelectric thick film at room temperature. *J. Mater. Chem. C* **3**, 1694–1699 (2015)
40. J.N. Li, D.W. Zhang, S.Q. Qin, T.Y. Li, M. Wu, D. Wang, Y. Bai, X.J. Lou, Large room-temperature electrocaloric effect in lead-free  $\text{BaHf}_x\text{Ti}_{1-x}\text{O}_3$  ceramics under low electric field. *Acta Mater.* **115**, 58–67 (2016)
41. J. Koruza, B. Rožič, G. Cordoyiannis, B. Malič, Z. Kutnjak, Large electrocaloric effect in lead-free  $\text{K}_{0.5}\text{Na}_{0.5}\text{NbO}_3\text{-SrTiO}_3$  ceramics. *Appl. Phys. Lett.* **106**, 202905 (2015)